remote sensing

MDPI

Article

Monitoring Rice Agriculture across Myanmar Using Time Series Sentinel-1 Assisted by Landsat-8 and PALSAR-2

Nathan Torbick [1,*], Diya Chowdhury [1], William Salas [1] and Jiaguo Qi [2]

[1] Applied Geosolutions, Newmarket, NH 03857, USA; dchowdhury@appliedgeosolutions.com (D.C.); wsalas@appliedgeosolutions.com (W.S.)
[2] Michigan State University, East Lansing, MI 48823, USA; qi@msu.edu
* Correspondence: ntorbick@ags.io; Tel.: +1-603-292-1192

Academic Editors: Nicolas Baghdadi, Xiaofeng Li and Prasad S. Thenkabail
Received: 22 December 2016; Accepted: 24 January 2017; Published: 1 February 2017

Abstract: Assessment and monitoring of rice agriculture over large areas has been limited by cloud cover, optical sensor spatial and temporal resolutions, and lack of systematic or open access radar. Dense time series of open access Sentinel-1 C-band data at moderate spatial resolution offers new opportunities for monitoring agriculture. This is especially pertinent in South and Southeast Asia where rice is critical to food security and mostly grown during the rainy seasons when high cloud cover is present. In this research application, time series Sentinel-1A Interferometric Wide images (632) were utilized to map rice extent, crop calendar, inundation, and cropping intensity across Myanmar. An updated (2015) land use land cover map fusing Sentinel-1, Landsat-8 OLI, and PALSAR-2 were integrated and classified using a randomforest algorithm. Time series phenological analyses of the dense Sentinel-1 data were then executed to assess rice information across all of Myanmar. The broad land use land cover map identified 186,701 km^2 of cropland across Myanmar with mean out-of-sample kappa of over 90%. A phenological time series analysis refined the cropland class to create a rice mask by extrapolating unique indicators tied to the rice life cycle (dynamic range, inundation, growth stages) from the dense time series Sentinel-1 to map rice paddy characteristics in an automated approach. Analyses show that the harvested rice area was 6,652,111 ha with general (R^2 = 0.78) agreement with government census statistics. The outcomes show strong ability to assess and monitor rice production at moderate scales over a large cloud-prone region. In countries such as Myanmar with large populations and governments dependent upon rice production, more robust and transparent monitoring and assessment tools can help support better decision making. These results indicate that systematic and open access Synthetic Aperture Radar (SAR) can help scale information required by food security initiatives and Monitoring, Reporting, and Verification programs.

Keywords: rice; Sentinel-1; food security; Myanmar; PALSAR-2; Landsat-8; random forest; classification; time series phenology

1. Introduction

Rice is one of the most important crops globally for food production, supporting livelihoods, and its role in global biogeochemical processes. Rice agriculture faces major challenges in the coming decade due to increasing resource pressures, severe weather and climate change, population growth and shifting diets, and economic development. More than 1 billion people depend on rice to support diets and livelihoods. However, the total accumulated area of rice has tapered off as available arable land is becoming scarce and competition for land uses evolve. This has resulted in intensified practices

for additional crop cycles and production amplifying water utilization and management to enhance harvested area and yield.

The majority of rice in today's world market is grown in South and Southeast Asia (India, China, Indonesia, Bangladesh, Thailand, Vietnam, Myanmar, Philippines) and many large rice producing nations import rice at times to meet demand [1]. With rice playing a critical role in food security and economics in this region, monitoring tools have come to the forefront of several initiatives, such as Asian Rice Crop Estimation and Monitoring (Asia-RiCE) and Group on Earth Observations Global Agricultural Monitoring (GEOGLAM) [2,3]. The overarching goals of these initiatives are to gauge production and potential risks to promote greater transparency and improved agricultural information. Satellite remote sensing has played a key role in supporting rice and food security initiatives, and the community has made significant progress. Current Decision Support Tools (DSTs), that include monitoring of crops operationally, are largely based on optical data, such as MODIS indices, combined with agro-meteorology metrics such as precipitation, temperature, solar radiation, and soil moisture. For example;

- Global Information and Early Warning System (GIEWS)
- Monitoring Agricultural ResourceS (MARS)
- CropMonitor
- CropWatch
- Space-based information for Disaster Management and Emergency Response (SPIDER)
- Famine Early Warning Systems Network (FEWSNET)

Traditionally, large-area rice mapping efforts rely on high temporal frequency optical imagery to map rice at regional to continental scales [4–10]. A popular approach uses high temporal frequency optical indices, from sensors such as MODIS, to extract phenological information and leverage the dynamic relationship among vegetation indices combined with masks. For example, the Land Surface Water Index (LSWI), Enhanced Vegetative Index (EVI), and Normalized Difference Vegetation Index (NDVI) generated from 8-day MODIS combined with masks such as land use and slope (e.g., [11–14]). By monitoring the pattern of these indices over time, metrics characterizing rice status is feasible. LSWI requires spectral information from the shortwave infrared band which is available at 500 m spatial resolution when using MODIS. Stress indices, such as Vegetation Condition Index [15], using MODIS, require information from thermal wavelengths which are generated at 1 km spatial resolution. Spectral matching techniques (SMT), decision trees, and wavelet approaches have also utilized similar scale data for large area rice mapping (e.g., [4–6,12–14]). Limitations when using these data are cloud coverage, spatial configuration and juxtaposition of paddies, and the relatively coarse spatial resolution of high temporal frequency optical sensors.

Landsat and its relevant derivative indices (i.e., LSWI, NDVI, temperature) have spectral bands sensitive to rice paddy conditions (i.e., [16–18]); however, phenological differences between scenes and low temporal frequency in the historical archives have limited mapping of rice at moderate scales over large areas. For example, 55 scenes are required for a single time period wall-to-wall mosaic of Myanmar. In cloud-prone regions such as South Asia, it is not uncommon to have months pass without a quality, cloud free (or low cloud) Landsat scene. Recent efforts have leveraged cloud technologies, such as Google Earth Engine and Amazon Web Services, to take advantage of moderate resolution Landsat archives and integrated computational processing. This has advanced mapping of rice extent over large regions at moderate scale, although the noted challenges remain given phenological dynamics, clouds, and repeat frequencies. A lack of quality, high temporal frequency optical imagery has limited moderate scale mapping of rice characteristics over large regions. Potentially, the fusion of the Landsat constellation with Sentinel-2 A and B will enhance our ability to operationally map crops at moderate resolution in a cost-efficient approach in the near future.

The all-weather capability, active sensing system that operates independent of sun illumination, and sensitivity to surface and subsurface characteristics make Synthetic Aperture Radar (SAR)

particularly useful for mapping rice in South and Southeast Asia. Many rice mapping techniques have been developed and utilization of temporal information has been a successful approach. For rice applications, microwave observations at the relevant configuration are sensitive to growth stages, biomass development, plant height, leaf-ground double bounce, soil moisture, and inundation frequency and duration [19–26]. During rice transplanting periods, the surface contribution of a rice paddy causes low backscatter. As plant tillering, biomass, and haulm develop, the backscatter response increases with more interaction and volume scattering causing a decrease in backscatter as the crop peaks and approaches harvest. This makes SAR particularly useful for mapping rice extent, inundation, and cropping intensity considering dynamic range and scattering mechanisms of the rice life cycle.

Historically, SAR applications for crop monitoring have been much fewer relative to optical data. The reasons for this include limited availability; no consistent, large-area acquisition strategies; poor quality digital elevation models required for processing; and complex data structures relative to optical data. Even the more progressive data acquisition plans have not met the requirements for large area operational monitoring of paddy attributes such as inundation duration. For example, the ALOS-1 acquisition strategy acquired an image in ScanSAR mode once every 46 days for the same area. With rice crops and typical rotations, it is not uncommon to have seasons less than 100 days making it impossible to confidently map conditions. While many SAR sensors have been utilized for rice mapping (i.e., ERS-1, ENVISAT ASAR, TerraSAR-X, Radarsat, ALOS-1), no options for cost-efficient, systematic, and continental scale data have existed until now.

Initiatives, such as AsiaRICE and GEOGLAM, are on a path to developing operational SAR (e.g., [26]); however, only since the launch of Sentinel-1 [27] has the science community truly had large area SAR acquisition at the scales needed to support food security programs. A coordinated shift by international space agencies has taken place with the goal to acquire systematic SAR acquisitions on a repetitive basis to support crop monitoring. Sentinel-1 now provides systematic C-band data at temporal frequencies far beyond previous collection strategies. As Sentinel-1A and B both become operational, the user community will have open access, operational C-band SAR at 6-day frequency for some priority regions. The proliferation of operational, moderate resolution (<30 m) and temporally frequent SAR will also lead to the next generation of Monitoring, Reporting, and Verification (MRV) tools that can help address climate change and agroforestry greenhouse emissions policies (e.g., [28]). The overarching goal of this research application was to develop and apply a rice monitoring framework using multiscale, moderate resolution imagery. Objectives of this effort were to (1) generate an updated land use land cover map using fused, multisensor imagery; (2) map rice extent, inundation, calendar, and intensity using moderate-scale and high temporal frequency Sentinel-1 observations; and (3) assess rice production in Myanmar and the ability of a multisensor approach to support operational monitoring of rice at moderate scales over a large area.

2. Materials and Methods

2.1. Study Areas

Myanmar

Myanmar has a complex and dynamic socioecological structure in which agriculture plays a central role. Myanmar is 676,578 km^2 in size and historically was a top rice producer; however, yield and production has not kept up with neighboring regions in the past few decades. Agriculture in Myanmar accounts for a large percent (50%–60%) of Gross Domestic Product and supports upward of 70% of the labor force [1]. The agriculture industry is sensitive to climatic change, weather variability, disaster, and economic stressors which present chronic risk. For example, milled production was reduced in 2015 by 400,000 metric tons due to flooding [29] and as a result, domestic prices increased and an export ban was temporarily put in place. Recent changes in political structure have re-emphasized agriculture as a focus industry to enhance livelihoods with technology infusion such

as improvements in irrigation infrastructure, genetic varieties, and management practices. Tools to accurately assess and monitor production, risks, and ecosystem services can thus play a major role in supporting policy, climate smart agriculture, and sustainable growth in Myanmar.

Most of Myanmar has a tropical climate with monsoon patterns along the coast (Köppen climate classification: Am, Aw) and a temperate dry hot period (Cwa) along the northern China and India borders. Temperatures range from 21 °C in the north to 32 °C along the coast. Rains typically start in May and retreat in November with portions along the Bay of Bengal, such as the Irrawaddy Delta receiving upwards of 3500 mm/year. Inland dryer regions north of Naypyitaw toward Mandalay average 1200 mm/year of rainfall. Due to the wide range in biomes, topography, and climate of Myanmar, the study area (country) was divided into four geographical zones for developing training data for the broad scale land classification. The representative regions used were, (1) northern Myanmar; (2) Central Dry Zone; (3) Irrawaddy Delta and (4) Tanintharyi.

Northern Myanmar terrain, which includes Kachin, northern Sagaing and northern Shan, is characterized by steep, rugged highlands at the foothills of the Himalayas. This region receives a moderate 1500–3000 mm of rainfall per year. South of this region, the Central Dry Zone, spread over Mandalay, southern Sagaing, Chin, and Western Shan, receives <500 mm of rainfall annually. This region frequently struggles with drought, requiring heavy irrigation of fields and has been developing irrigation infrastructure as part of the country's food security goals. Further south of this is the Irrawaddy Delta which the largest rice production region in the country and major production hot spot in South Asia. Agriculture here is largely reliant on the rain season, and producers often struggle with monsoon driven flooding, receiving over 3000 mm of rainfall per year. Lastly, the Tanintharyi region, located on the Kra Isthmus, is characterized by its coastal terrain. The region receives a large amount of rainfall, with some parts, such as Dawei, receiving over 5000 mm of rainfall annually. The primary crops grown in this region are rice, rubber, and fruit crops.

Typically, the main rice crop is sowed between May to early June, grows until September, and is mostly harvested during November with some regions trailing into December harvests (Table 1). However, tremendous local variability can exist creating challenges for operational monitoring. The vast majority (>75%) of rice is produced during the main wet season in Myanmar. A second rice crop, if amenable conditions exist, can potentially be sowed during November with harvest by May the following year. Maize, potatoes, wheat and a mix of cash, food, and rotation crops can be grown outside of the main rice season. Rotations, failed crops, fallow land use, and yield can vary tremendously spatially, within season, and season-to-season making assessment very challenging. Little to no data is available in an open access environment due to the previous political structure and level of capacity. The Food and Agricultural Organization's (FAO) GIEWS reported that 28,900,000 tonnes of paddy rice were produced in 2014.

Table 1. FAO Myanmar rice crop calendar.

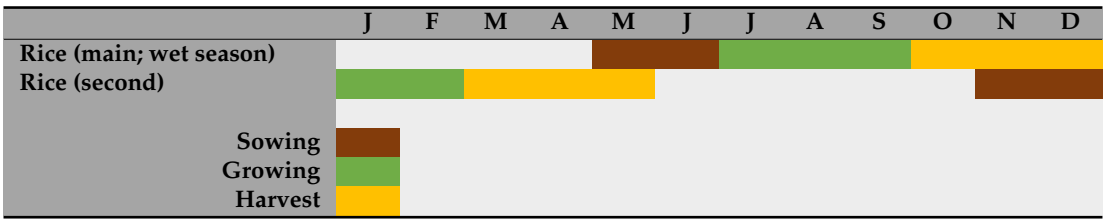

2.2. Data Processing

2.2.1. Landsat-8 OLI

A total of 55 Landsat 8 Operational Land Imager (OLI) scenes were used to provide surface reflectance λ and optical indices to characterize the landscape into broad categories (Figure 1). All Landsat data were obtained from United States Geological Survey (USGS) Earth Explorer.

L8SR code was used to generate surface reflectance and masking to screen out poor quality Landsat pixels due to clouds and shadows. The L8SR approach [30,31] builds off the lineage of Landsat 5 and 7 preprocessing work flows [32–36]. The best available imagery from 2014 and 2015 was selected based on phenology and cloud cover. A set of well-established indices were used to help classify the landscape. Indices are less sensitive to image-to-image noise, viewing geometry, and atmospheric attenuation, making them particularly advantageous over reflectance products when using large area mosaics covering scenes spread over multiple paths, rows and dates.

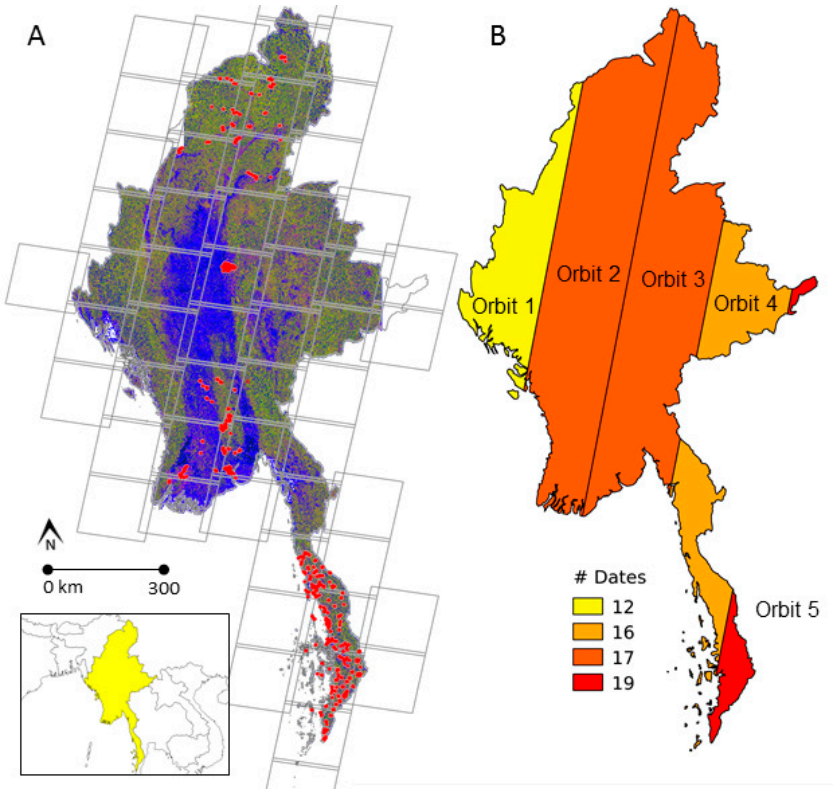

Figure 1. (**A**) Location of training polygons (red) overlaid on 2015 PALSAR-2 (Red: HH, Green: HV, Blue: HH/HV^2) Mosaics with Landsat World Reference System path rows shown; (**B**) Orbit paths for Sentinel-1 with heat map of image frequency for 2015.

This research application used the Normalized Difference Vegetation Index (NDVI; Equation (1)) [37,38], a useful metric of greenness and vigor across a landscape. The Land Surface Water Index (LSWI; Equation (2)) given its sensitivity to water or equivalent water thickness and leaf moisture has been successfully applied for mapping inundation, forest characteristics, and agricultural landscapes [39]. The Soil-Adjusted Total Vegetation Index (SATVI; Equation (3)) has demonstrated utility in mapping senescent biomass, ground residue, plant litter, and surface conditions while compensating for varying soil brightness and background artifacts [40].

$$\text{NDVI} = (\rho_{\text{NIR}} - \rho_{\text{R}})/(\rho_{\text{NIR}} + \rho_{\text{R}}) \quad (1)$$

$$\text{NDVI} = (\rho_{\text{NIR}} - \rho_{\text{R}})/(\rho_{\text{NIR}} + \rho_{\text{R}}) \quad (2)$$

$$\text{SATVI} = (((\rho_{\text{SWIR1}} - \rho_{\text{R}})/(\rho_{\text{SWIR1}} + \rho_{\text{R}} + L)) \times (1 + L)) - (\rho_{\text{SWIR2}}/2); L = 0.5 \quad (3)$$

2.2.2. PALSAR-2

Wall-to-wall L-band measurements were used to help classify the landscape into broad land use land cover classes. The Advanced Land Observing Satellite (ALOS-2) carries the Phased Array type L-band Synthetic Aperture Radar (PALSAR-2) instrument building on the lineage of ALOS-1 PALSAR-1 and Japanese Earth Resources Satellite 1 (JERS-1). ALOS-2 orbits at an altitude of 628 km in a Sun-synchronous pattern. In this study, PALSAR-2 backscatter mosaic products were obtained from JAXA for the year 2015. Backscatter mosaic products are distributed as $1^\circ \times 1^\circ$ tiles, at a resolution of 0.8 arcsec (~25 m) ground resolution. A total of 200 scenes were used to create a wall-to-wall map for Myanmar (Figure 1). Data are ortho-rectified and slope corrected by JAXA before being distributed as Digital Number (DN) values along with ancillary files such as observation date, local incidence angle, and mask information required during pre-processing. The DN values for each polarization HH; HV (horizontal transmitting, horizontal receiving; horizontal transmitting and vertical receiving) were converted to sigma naught (σ° dB) backscatter coefficients using Equation (4)

$$\sigma^\circ = 10 \log 10\langle DN^2 \rangle + CF; \; CF\text{–Calibration Factor } (-0.83 \text{ dB}) \quad (4)$$

2.2.3. Sentinel-1

C-band measurements were used to help classify the landscape and characterize rice paddy attributes. Sentinel-1A carries a C-band imager at 5.405 GHz with an incidence angle between 20° and 45°. The platform follows a Sun-synchronous, near-polar, circular orbit at a height of 693 km. The 1A platform has a 12-day repeat cycle at the equator. The Sentinel-1B platform was launched in April of 2016 and is now actively collecting measurements. Now that 1A and 1B are operational, C-band imagery are available once every 6 days in some priority regions as part of the European Space Agency (ESA) data observation strategy while some regions will be less frequent. Sentinel-1 collects in four modes, namely Stripmap (SM), Interferometric Wide Swath (IW), Extra Wide (EW) and Wave, with varying resolutions, extents, incidence angles and polarizations. This study focused on using conflict free IW mode data acquired between 14 February 2015 and 7 May 2016. This mode observes in single and dual polarization VV; VH (vertical transmitting, vertical receiving; vertical transmitting, horizontal receiving) with a 250 km footprint in range direction. All data are freely available from the ESA Data Hub and mirrored at the Alaska Satellite Facility (ASF).

Data were obtained as Standard Archive Format for Europe (SAFE), which contains general product information in XML, for the entire region using the open access data archives. Annotated data sets hold metadata on the main characteristics including acquisition, image properties, polarization, Doppler information, swath merging, calibration, and geographic location. SAFE products were obtained as Ground Range Detected (GRD), which have already been focused, multilooked, calibrated and projected in ground range. We performed comparisons and sensitivity testing between GRD and Single Look Complex (SLC) that included combinations of multilooking and speckle filtering using image differencing and examination of algorithms at training sites. Given that ESA began observations using GRD, no improvements were found in products at training sites using SLC in correspondence with the approach executed in this effort, and the tradeoff in processing requirements, we focused on GRD for a larger (time and space) archive of images. Data were terrain-corrected, normalized, and calibrated using local incidence angles and cosine correction before converting to sigma naught (σ° dB) for mapping and analyses. A nominal 20 m spatial resolution was executed in this effort for final products considering size, speed, connectivity, and formats when sharing data with local and international partners. Layover and shadow map were generated for post processing using a Shuttle Radar Topography Mission version 4 Digital Elevation Model. A total of 39 Sentinel-1A images were required for a single time period, wall-to-wall mosaic of Myanmar. Sentinel-1 data were divided into five unique orbits and mosaicked by cycles. For time series analysis, a total of 632 images were used, across all orbits and cycles (dates) (Figure 1).

2.3. Mapping Approach

2.3.1. Land Use Land Cover Mapping

The first objective was to create an updated land use land cover map for identifying broad landscape classes including built, forest, shrub, water, and crop. Training data were created using multiple sources of data. Two brief field campaigns were conducted in November 2015 and January 2016 that traversed major travel routes between Yangon, Naypyitaw, and Mandalay. These field campaigns included limited farmer surveys designed to help calibrate the imagery and guide decisions regarding tuning of algorithms. At a subset of farms, we surveyed hydroperiod management, cropping intensity, estimated calendar, and general conditions while taking geofield photos. In an effort to support open calibration and validation of satellite mapping, our team has been growing an online archive of field-level photos using a GPS-enabled camera (Figure 2). All geofield photos are linked to shape files or keyhole markup language (KML) files to store, display, and share photos. These photos are available for viewing and sharing www.eomf.ou.edu/photos [41]. The archive for Myanmar now has 1367 open access geofield photos.

Google Earth high resolution imagery and the geofield photos were used to create polygons to train the classifier following [42]. We developed randomly stratified training data in four main regions (1) northern Myanmar; (2) Central Dry Zone; (3) Irrawaddy Delta and (4) Tanintharyi. As described, these areas represent a range of bioclimatic and land cover/use conditions. The four regions were chosen to ensure regional sensitivity of classification models that also considered repeat frequencies and phenology. Training polygons were dispersed across these landscapes and considered a variety of landscape conditions such as patch size, slope, density, class balance, elevation, and distance to urban areas, to build robust training and validation assessment. A total of 459 polygons were carefully digitized across the study regions (Table 2). For each region and potential combination of image data sources, an error matrix was generated using withheld out-of-sample points.

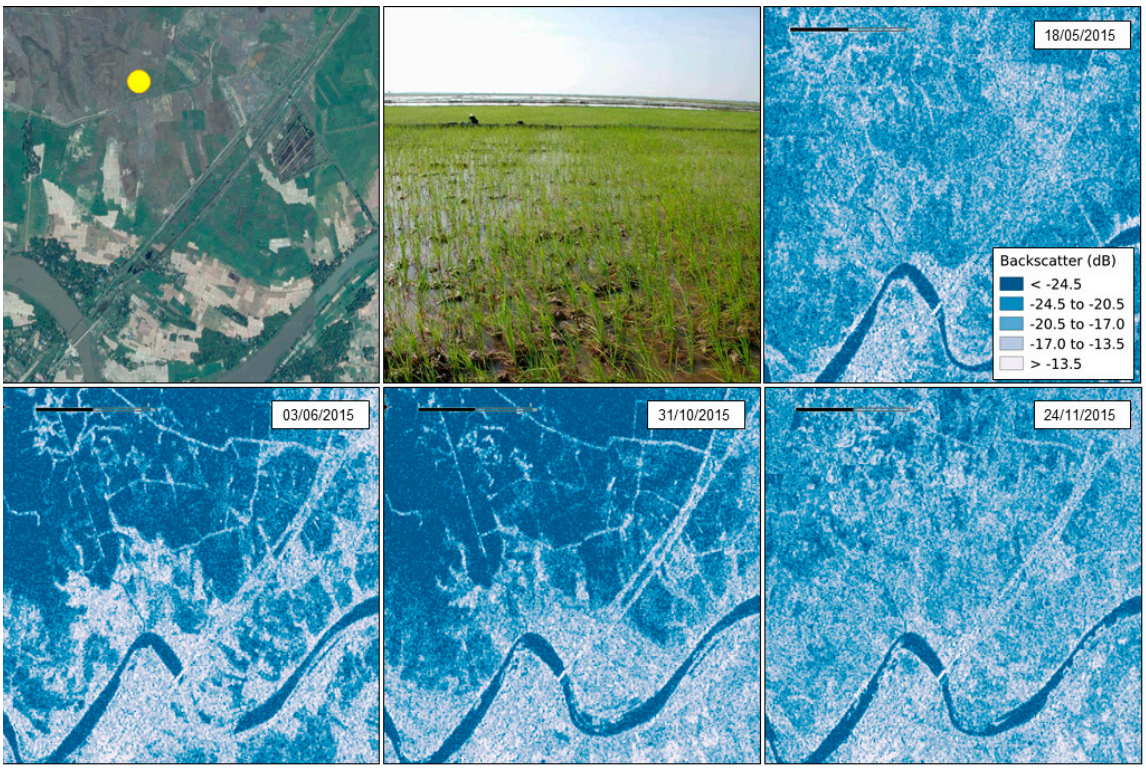

Figure 2. Example geofield photo and time series Sentinel-1 backscatter dB illustrating dynamic inundation (blue tones).

Table 2. Characteristics of training data used for the Classification And Regression Tree to generate a broad class map.

Class	# of Polygons	# of Pixels	Min Patch (Ha)	Max Patch (Ha)
Crop	100	72,686	1.36	695.66
Water	92	76,888	0.62	1125.40
Forest	100	903,064	1.31	4862.90
Shrub	73	14,900	0.16	207.34
Built	94	68,822	2.97	325.34

A Classification and Regression Tree (CART) routine was applied to generate the updated Land Use Land Cover (LULC) map using a stacked data cube (Figure 3). The data cube was created from stacking the preprocessed Landsat-8, PALSAR-2, and Sentinel-1 observations following the lineage of [42]. The ensemble, machine-learning, random forest algorithm [43] was used as the initial classifier with the training data. A random forest is generated through the creation of a series of CARTs using bootstrapping, or resampling with replacement. Random forest is a flexible and powerful nonparametric technique that many mapping applications have recently implemented for a range of studies including mapping crops [44–46], wetlands [47,48], canopy height [49], algal blooms [50], urban sprawl [51], biomass [52], plantations [42], and many other thematic areas.

For random forests as applied here, a number of decision trees were built and each time a split in a tree is considered, a random sample of m ($m < p$) predictors is chosen as split candidates from the full set of p predictors. In this case, m:$\sqrt{p}$ was applied and this process can be seen as reducing the variance of the resulting trees. A large tree with more splits may have small bias but lead to higher variance that is challenging to interpret. A small tree with less splits may result in more bias but have lower variance and more straight forward interpretation. With random forest, it is possible to build regression trees that are large, and then prune to determine which subtree gives the lowest tree error rate. Random forest has the ability to treat small and large p problems, high-order interactions, and correlated predictor variables. An advantage of random forest is the easy integration of multiscale and multimodal input variables, and it includes a robust ability to handle large and diverse datasets efficiently.

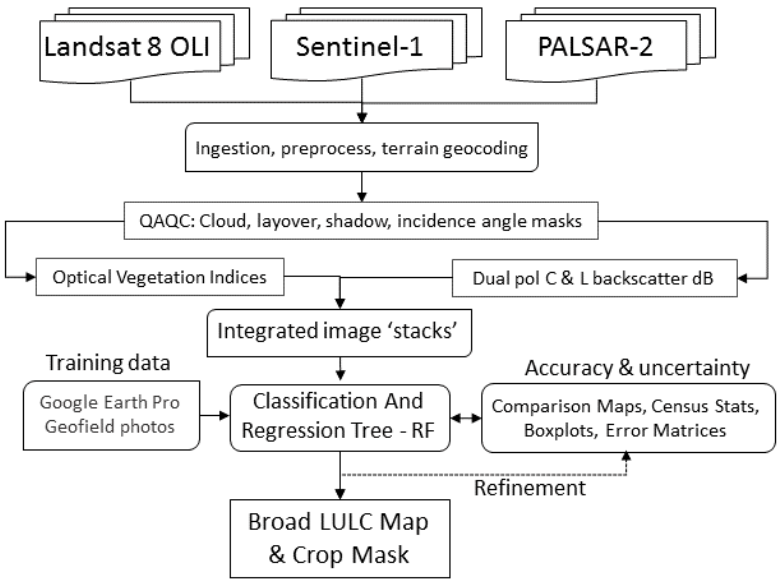

Figure 3. Work flow of multiscale mapping for broad updated land cover land use map.

A complementing set of accuracy assessment and validation statistics were used to evaluate the workflow and mapping outcomes. Out of bag (OOB) or "withheld" samples were used to construct the error matrices and cross-validate broad scale mapping outcomes. These accuracy assessment metrics along with box and whisker plots provide an assessment of mapping capabilities across the four different geographic regions and an understanding of which inputs in the data cube were driving splits in the CART. Limited open access government census statistics are available in Myanmar. For this research, we used 2015 census statistics to compare harvested area by State. Diligent treatment of the data was performed following best practices. We emphasize the extreme lack of availability as a driving force behind this work. At the national scale, more recent census estimates are available.

2.3.2. Time Series Analysis

A time series analysis (TSA) was carried out on dense time series Sentinel-1 to extrapolate unique indicators tied to the rice life cycle, and refine the broad scale map (Figure 4). The outcomes of the TSA were information on rice extent, inundation, calendar, and cropping intensity. The indicators of the rice life cycle are attributes associated with field management, inundation, and growth stages. When these different attributes are combined, a more thorough understanding of production and risk assessment is feasible. Further, an approach that was robust and transferable was desired to support scaling efforts for large area assessment and monitoring.

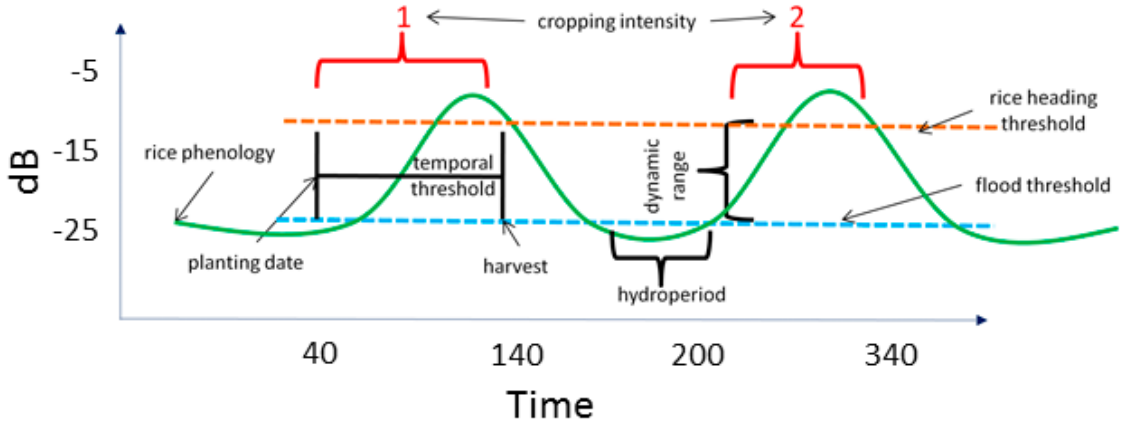

Figure 4. Conceptual Sentinel-1 double rice signature with key indicators highlighted from management (i.e., inundation) and rice growth stages (i.e., biomass development and dynamic range).

Several studies have detailed rice backscatter responses for varying wavelengths, polarizations, incidence angles, scales, and field properties [20–26]. Recently, [53] found VH polarization Sentinel-1 data to be sensitive to rice cultivation in the Mekong Delta. Reference [26] provides a thorough review of the finer details among SAR bands, polarizations, and rice biogeophysical attributes. In general, irrigated rice paddies are inundated prior to emergence of the crop due to sowing or transplanting, which results in a low radar backscatter response. As rice crops grow and gain in biomass from tillering, pinnacle formation, and flowering, the backscatter response increases proportionally with more interaction from double-bounce and direct volume scattering mechanisms until crops head. After ripening and near harvest, paddies are usually drained if still flooded or decrease in saturation and moisture due to mature haulm and leaf area which causes a shift toward a leveling off or decline in backscatter. A backscatter response for rice at a nominal incidence angle can capture dynamic range on the order of 8 to 10 σ° dB when timing of overpasses correspond to the 'valleys and peaks' of a rice signature [8,20,25]. Thus, using dense time series data tuned to these rice life cycle stages is essential to mapping rice attributes and field conditions.

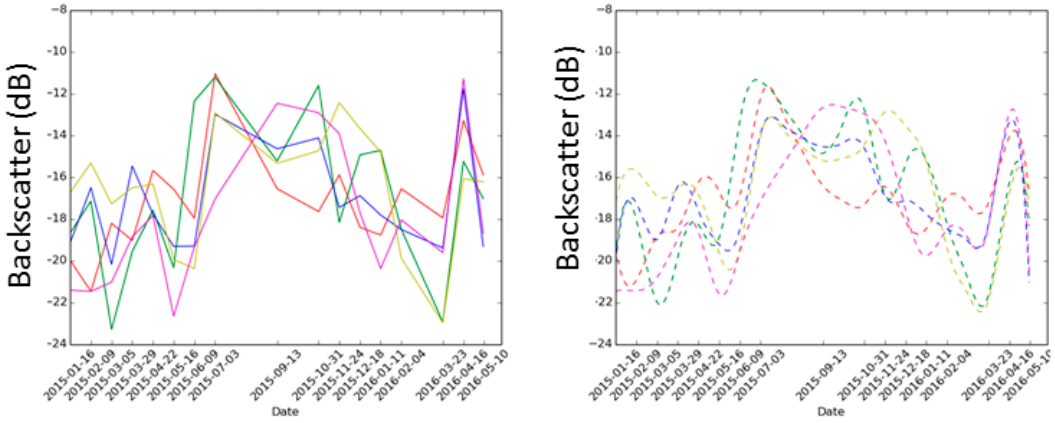

Figure 5. Example interpolated and smoothed time-series Sentinel-1 shown for rice pixels in northern Myanmar region.

TSA was carried out using all available Sentinel-1 IW Mode data between 14 February 2015 and 7 May 2016. To map crop calendar, we followed the linage of Rojas et al [15] that have successfully used optical indices (i.e., NDVI) and phenological patterns to note seasonality. Due to the noise, inherent in SAR data, and temporal gaps in this dataset, various interpolation and smoothing techniques, such as Savitsky–Golay [54], Whittaker [55], cubic splines, and linear, were evaluated to create a more complete temporal backscatter signature (Figure 5). Many studies have described the strengths and limitations of these different smoothing techniques (e.g., [56–58]). For calendar mapping, peak VH backscatter was identified using maximum value. The previous minimum (valley) before upward inflection that is caused from biomass development was identified as an emergent or transplant date. Other peaks in the time series that are at least 20% of the absolute maximum were searched as a metric of cropping intensity (i.e., single, double, triple). A set of temporal thresholds were tested and integrated to ensure unrealistic outcomes, which were flagged and excluded. In this research calendar, dates were constrained to eliminate any crop cycles shorter than 80 days, and cropping intensities larger than two during the main crop periods. These parameters were selected based on a conservative deduction from local field surveys, limited census statistics, and expert knowledge.

A phenologically sensitive, thresholding approach was applied to identify inundated area in an effort to develop hydroperiod metrics. Hydroperiod is the frequency, duration, and timing of inundation. These rice field characteristics can be used to help understand irrigation, calendar, rotations, and intensity patterns. Training data based on identified field conditions in imagery, was used to define a set of thresholds. Figure 2 illustrates Sentinel 1-A backscatter before, during, and after the rice growing season. The trend of agricultural areas transitioning to inundation is apparent, with backscatter values appearing as darker tones in the time series. Incidence angle impacts were considered during the development of thresholds although, using a robust TSA, the difference between near range and far range (within orbit paths) in affecting the threshold values was minimal in this application. Backscatter signals from open waterbodies, wetlands, and inundated fields were also compared across time and seasons to get a sense of dynamics tuned to rice development. Different iterations were tested and compared against Google Earth high spatial resolution imagery, geofield photos and farmer surveys. A set of hydroperiod metrics was derived including percent of time inundated and presence of standing water before emergence and/or during sowing. Finally, by combining measures of extent, inundation, calendar and intensity in a logical, robust, and consistent manner, a more comprehensive understanding of rice production was possible in an operational context (Figure 6).

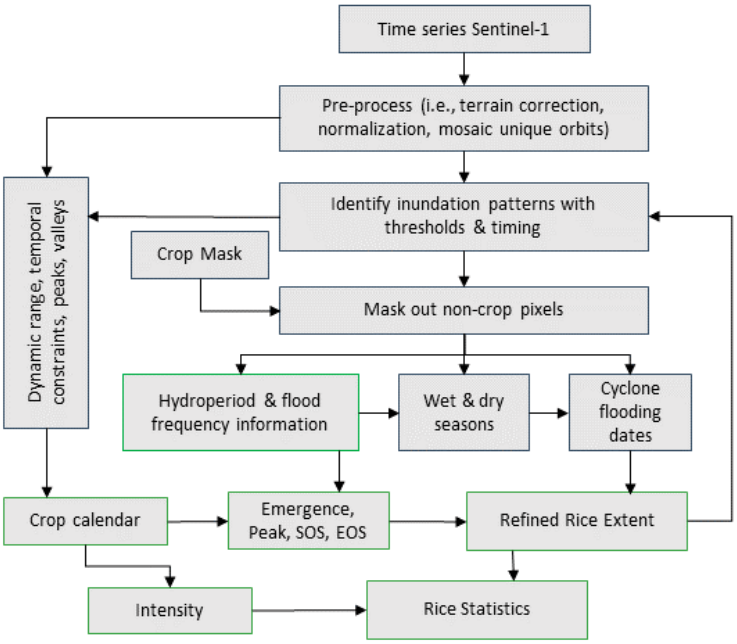

Figure 6. Work flow for refining rice information products (extent, hydroperiod, calendar, intensity, harvested area) using dense time series Sentinel-1, masks, and phenological analysis.

Rice accuracy assessments were performed using agricultural census statistics and comparison maps. In this study, temporally consistent (2015) census statistics and imagery were compared at the "State" level. Averages across previous years (i.e., mean area harvested 2009–2014) were also evaluated. Use of these government census statistics needs to be done cautiously given the lack of transparency, gaps in recent availability, and shifts in political boundaries. Total harvested area for Myanmar is made available by FAO on a national scale routinely while at finer administrative units, gaps can exist. Other maps include International Rice Research Institute (IRRI) and European Space Agency (ESA) products using MODIS and MERIS, respectively. However, comparison is not one-to-one given the vastly different resolutions of the data, timeframes, geographic coverage, and ontologies of the respective datasets.

3. Results and Discussion

3.1. Mapping Land Cover Land Use

Up-to-date land use land cover data are not widely available for Myanmar and this effort represents one of the few datasets available at moderate resolution covering the entire region. The example box and whisker plots highlight the strength of a given sensor for a specific class and/or season. Figure 7 illustrates Sentinel VH differences between northern Myanmar and Irrawaddy Delta with distinctions in crop inundation. Northern Myanmar tends to be dry with more scattered rainfed rice relative to the delta as evident by the response in backscatter being 8–10 dB lower on similar dates. In northern Myanmar, crops were more likely to be confused with forest and shrub in the initial classifications as compared to the delta where crop and water are more likely to get confused if only using single time imagery during the main wet season. Landsat NDVI separated classes well in northern Myanmar, excluding built and crop due to the use of Landsat from the dry season (no clouds) when crops are not grown and fields are often fallow. In the delta, crop and water are more likely to get confused when only using single time imagery due to abundance of rice crops in this region and the flooding of paddies typical of this crop type. PALSAR-2 strengths were in identifying inundated area given its long wavelength and penetration capabilities. However, only having one time period from PALSAR-2 limits its applicability for monitoring phenology.

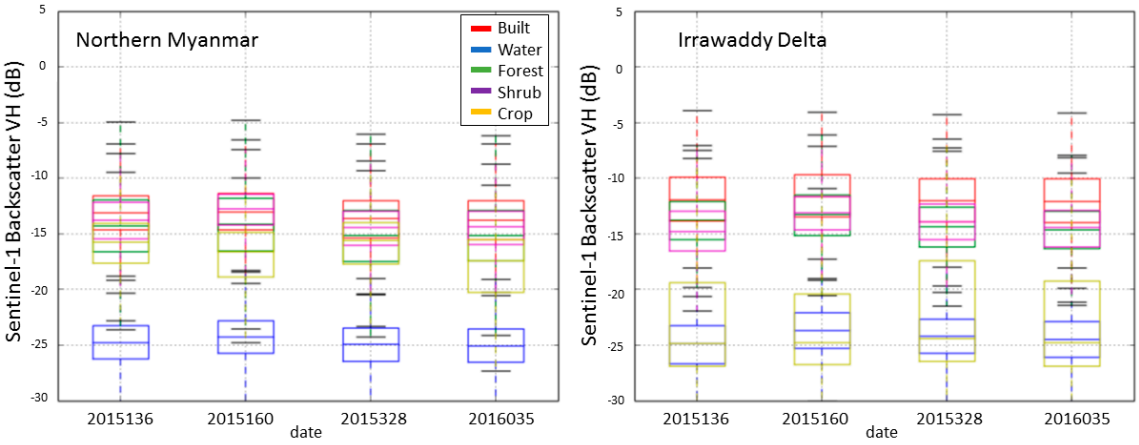

Figure 7. Sentinel-1 Vertical transmit Horizontal receive dB box and whisker plots for two training regions highlighting differences in irrigated rice response.

No one index, polarization or sensor separates all classes with very high accuracy across all four training regions. Information from complementing wavelength domains (C, L, VIS, NIR) were fused for improved classification. As noted, the use of random forest enables easy integration of a multimodal data cube and takes advantage of statistical differences among the different input sources to create nodes for separation. The withheld sample error matrices emphasize these results. The combination of Sentinel-1 and PALSAR-2 had the lowest cross-validated, overall accuracy and kappa of 0.82 and 0.71, respectively, in the Irrawaddy region. The fusion and use of L-band and optical data has been found advantageous in other studies (e.g., [42]) and again here. Our results have a mean out-of-sample kappa of over 90% for all four stratified regions, with northern Myanmar having the highest accuracy and Tanintharyi having the lowest largely due to the high patchiness of the landscape and mosaic mixed vegetation and cropland cover classes (Table 3).

Table 3. Example Tanintharyi error matrix for a broad class map using fused Landsat-8, PALSAR-2, and Sentinel-1 imagery where the withheld kappa statistic was 0.92.

		Crop	Water	Forest	Shrub	Developed
Tanintharyi	**Crop**	35,962	1	1	0	23
	Water	0	27,265	0	0	1
	Forest	5	2	794,587	24	0
	Shrub	0	0	122	11,124	0
	Developed	43	9	4	0	36,903

The combination of Landsat-8 OLI-derived indices NDVI, LSWI and SATVI along with PALSAR-2 HV polarization generated the best overall broad class map as determined by the box and whisker plots (Figure 8), error matrices, and visual inspections of classifications (Figure 9, Table 4). This initial classification product identified 186,701 km^2 of cropland or approximately 27% of Myanmar which is slightly higher but in line with trends estimated by the FAO and the World Bank (Figure 10). This area also likely includes a mix of scrub-shrub, mixed mosaic land uses, and fallow land use as the extent of what is actually cultivated in a given year is not maximized arable area in Myanmar. The FAO estimated 19.3% in 2013 with a 20% rise since 1995 following three decades of flat growth. The Ministry of Agriculture and Irrigation (MOAI) estimates the rice area as 34.1% of the total cultivated area in 2014.

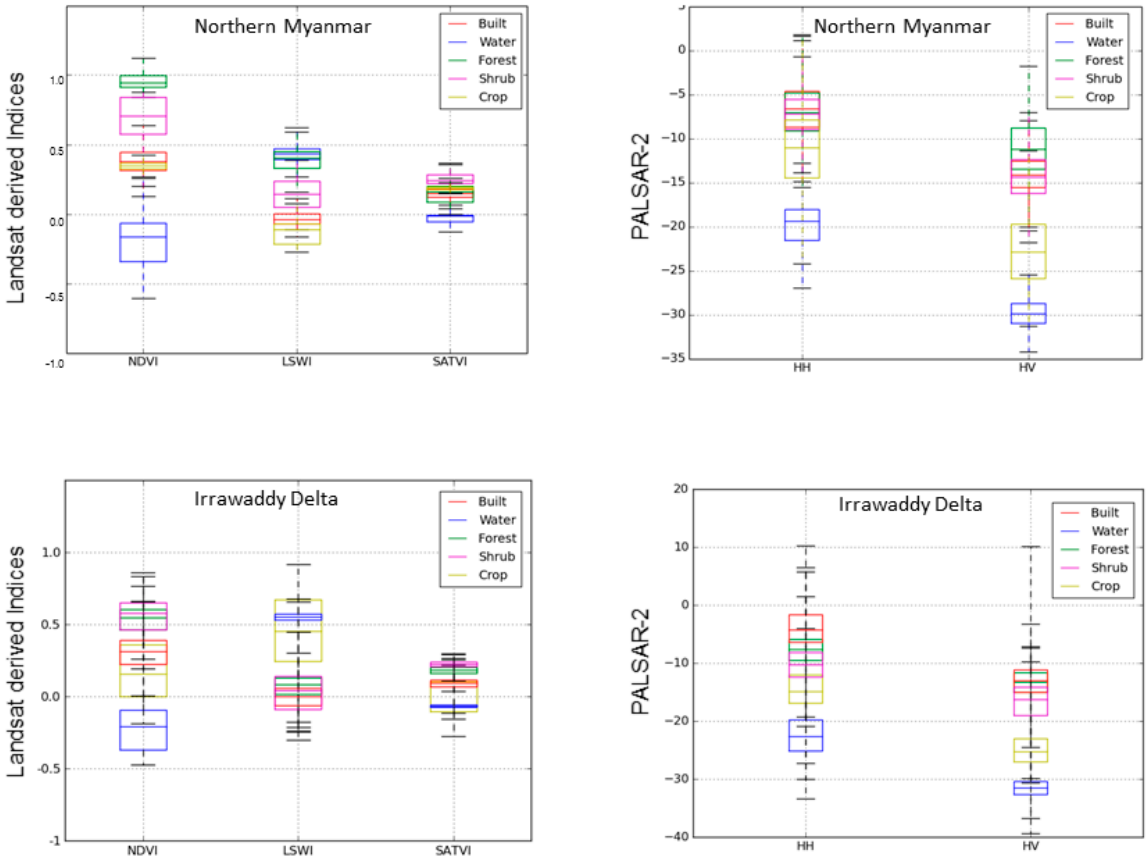

Figure 8. Landsat-8 indices (NDVI, LSWI, SATVI) and PALSAR-2 (HH, HV) backscatter responses for two selected training regions showing overlap and/or separation between the two regions among the remote sensing observations.

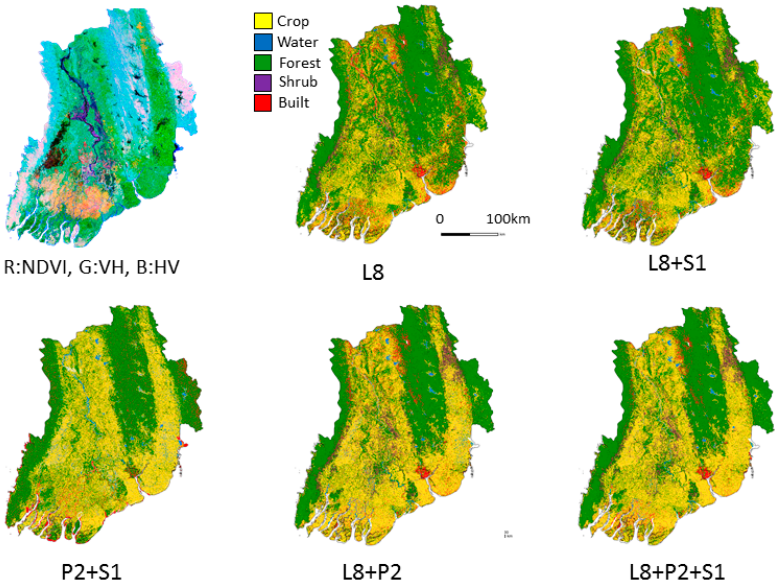

Figure 9. False color (R: Landsat NDVI, G: Sentinel-1 VH, B: PALSAR-2 HV) and classification outcomes for Irrawaddy Delta using different combinations of Landsat-8 OLI (L8), Sentinel-1, and PALSAR-2.

Table 4. Example mean withheld out-of-sample kappa values for Irrawaddy Delta combinations of imagery data and classifications.

Landsat-8	0.94
Landsat-8, PALSAR-2	0.95
Landsat-8, Sentinel-1	0.94
Sentinel-1, PALSAR-2	0.71
Landsat-8, Sentinel-1, PALSAR-2	0.95

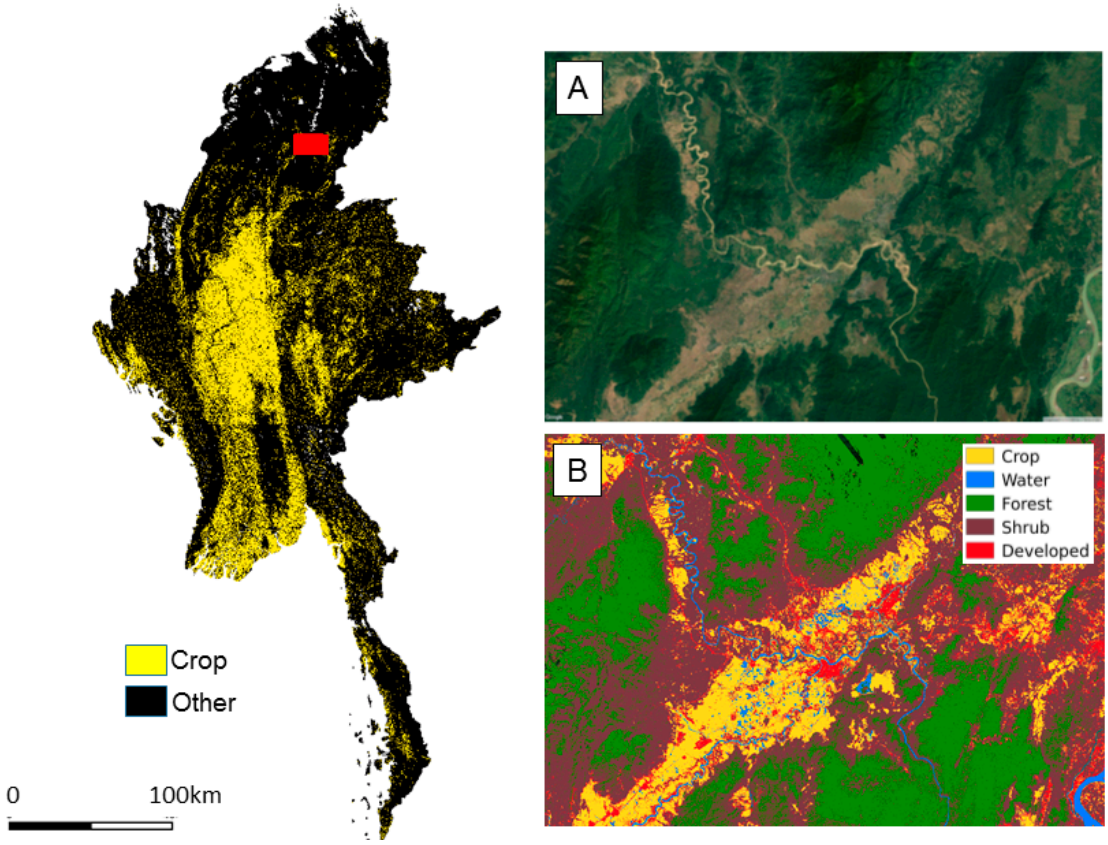

Figure 10. Updated (2015) crop mask for Myanmar using integrated optical and SAR inputs and example zoomed in snapshot (**A**: Google Earth, **B**: Classification) of Mogaung region within Kachin State.

3.2. Mapping Inundation and Refining Rice Extent

Inundation was mapped using a thresholding approach that also considered incident angles, seasonality, and rice stages. By fusing the inundation information with crop masks a more detailed analysis of rice and irrigation was possible. Rice systems vary spatially across Myanmar and can undergo tremendous variability with the magnitude and timing of inflection in Sentinel-1 requiring robust approaches to accurately map inundation. For example, Sentinel σ° VH differences between northern Myanmar and Irrawaddy Delta were detectable due to northern Myanmar receiving less rainfall with landscape conditions being more patchy, scattered rainfed rice relative to the delta region. The pixel-based TSA constrained inundated rice by detecting flooded conditions that were followed by increasing backscatter and a minimum dynamic range. Additionally, inundation and rice area was constrained by using temporal intervals of growth stages, crop cycles tuned to seasonality (wet season and dry season), and the crop mask. This was an effective method to identify rice extent and hydroperiod (the duration of flooding, timing of inundation, and/or frequency of inundation).

Relatively high frequency of inundation was observed in the Irrawaddy Delta, including the states of Irrawaddy, Rakhine, Yangon and Bago. Inundation of this region is shown in Figure 11 on ten

dates from the 2015 time-series. The Delta region is one of the largest rice producing hot spots in the country with a majority fed by interlocking channels of water tributaries. Pockets of aquaculture were also detected and differentiated using the patterns of inundation tuned to seasonality of rainfall and crop phenology. The regions with pockets of aquaculture are within the states of Irrawaddy, Rakhine, Yangon and Bago. Potentially these aquaculture patterns can create confusion with rice cycles if the time series of Sentinel-1 has gaps during key growth stages. Irrigation patterns in the central Dry Zone (including states of Mandalay, Magway and Sagaing) were visible in the time series. Due to low rainfall levels and persistent drought in recent years, portions of this region have irrigation infrastructure to support rice production which was observed (Figure 12).

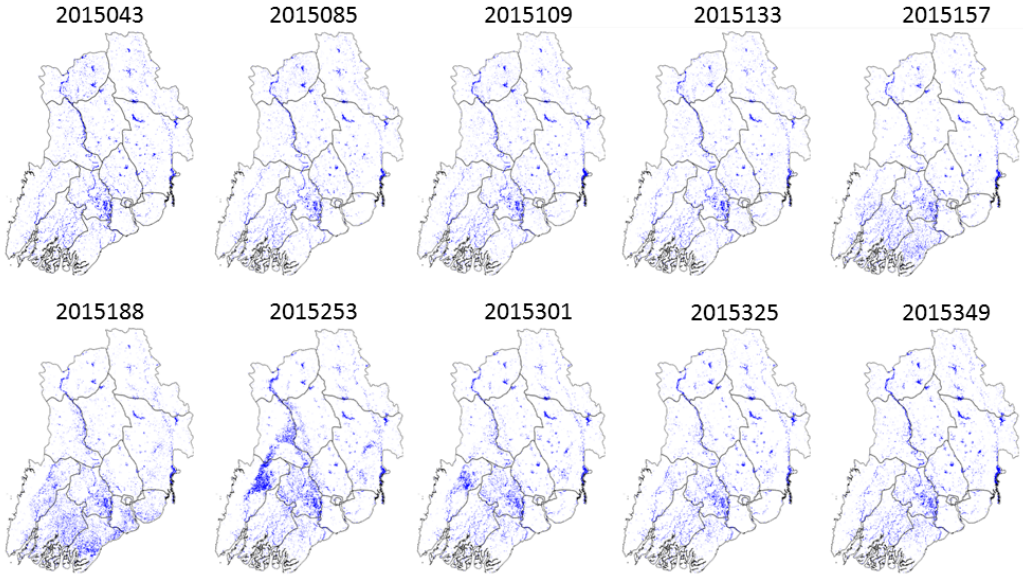

Figure 11. Inundation patterns in the Irrawaddy Delta region of Myanmar using dense time series Sentinel-1.

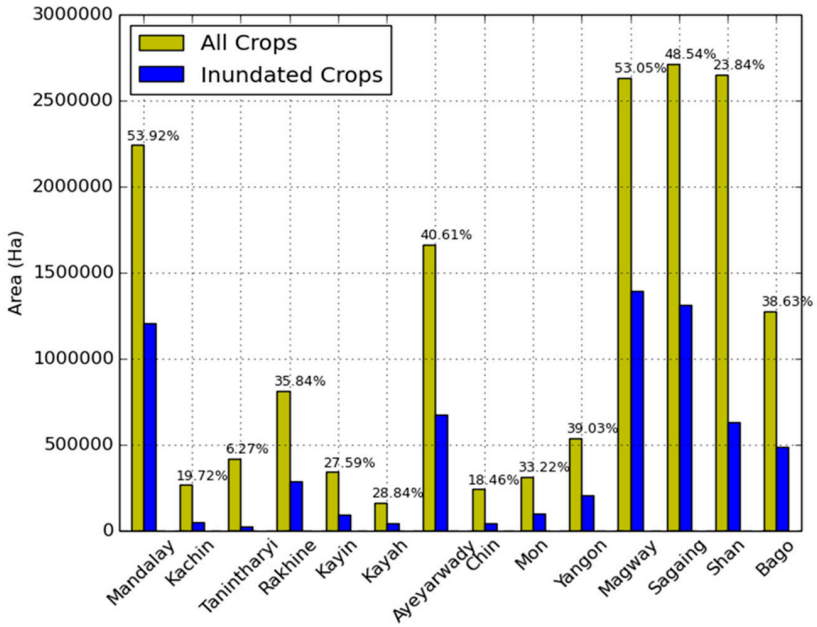

Figure 12. Inundation patterns in the Irrawaddy Delta region of Myanmar using dense time series Sentinel-1.

One of the limitations of C-band Sentinel-1 SAR, as used in this application, was mapping of inundation below full or dense crop canopies. Sensors, such as PALSAR-2 or planned P-band BIOMASS, with longer wavelengths, are more capable of extracting below canopy inundation signals given the longer wavelength and penetration capability. However, the systematic temporal repeat frequency of Sentinel-1 enables for mapping inundation dynamics at field scales far beyond what was previously possible. For example, PALSAR-1 and ENVISAT ASAR had repeats on the order of 46 and 35 days, respectively. As both Sentinel-1A and 1B are now operational, the amount of hydroperiod information (i.e., frequency, duration, timing) potentially available to the science community, especially in cloudy regions such as South Asia, is at spatial and temporal scales required to meet the needs of most food security programs and assess impacts of drought earlier in the season. Recently, [59] showed improvement in early season mapping with Sentinel-1 in a small area of France. With the short latency period, open access data, and operational acquisition strategy over land, near real-time estimates of the planted area are feasible. This is one critical variable desired by food security monitoring programs and DSTs. By assessing deviations in extent or, for example, impacts of a cyclone or humanitarian crisis, impacts on production can be rapidly gauged to support decision making. This approach is robust, systematic, as well as transparent which are requirements of most food security initiatives such as GEOGLAM.

3.3. Mapping Crop Calendar and Intensity

Crop calendar, keying off inundation, dynamic range, and temporal constraints, was able to accurately distinguish the major stages of the rice life cycle including emergence, start-of-season, peak, and end-of-season. By aggregating these features over time, cropping intensity was mapped on a pixel level. The typical practice of inundating rice fields prior to sowing/transplanting results in a noteworthy low backscatter value followed by a large dynamic range in SAR backscatter signal between emergence and peak season. This feature is a powerful attribute if the time series is dense enough. Results for average calendar dates for main crop season per state can be seen in Figure 13. Comparison to FAO GIEWS shows strong correspondence for the wet season rice calendar dates between March and November, and dry season from November to March. The wet season dates align well with our crop calendar results for the main crop which represents the majority of production (>75%). Our cropping intensity results show an average of 142.4% for all of Myanmar, which is slightly lower than the 2013–2014 FAO value of 160.3%.

Potentially, this approach and ability to monitor rice status, given the short latency of Sentinel-1, can help respond to disaster and food security decision making in Myanmar. With a better understanding of rice growth stages, calendar, and inundation cycles, the impacts of floods can be better assessed in regions where rapid, robust, and transparent information is lacking. For example, in July of 2015, heavy rains from Cyclone Komen caused widespread and substantial damage during key sowing periods in many regions of Myanmar including Chin, Rakhine, Ayeyarwaddy, Yangon, Sagaing and parts of Bago. Figure 13 shows Start Of Season (SOS) dates with mean dates around Day Of Year (DOY) 200, indicating delayed and/or re-planting likely occurred due to Cyclone Komen flood damage. Assessment of food security was challenging given the lack of readily available information with estimates showing a 4% drop in rice production [1]. Chin and Rakhine were especially hard hit given the highly vulnerable populations in these States. Many farms were able to replant; however, a lack of information has been reported as a major obstacle [1]. For example, MOAI estimated that 99% of rice area was replanted initially and that number has subsequently been revised to <50% by the Myanmar Rice Federation. Further field investigations have shown many regions replanted black gram, cowpea, and maize instead of paddy rice. Figure 14 shows mean calendar dates for the main wet season crop and highlights the Central Dry Zone from Naypyitaw north to Mandalay and Shwebo production areas.

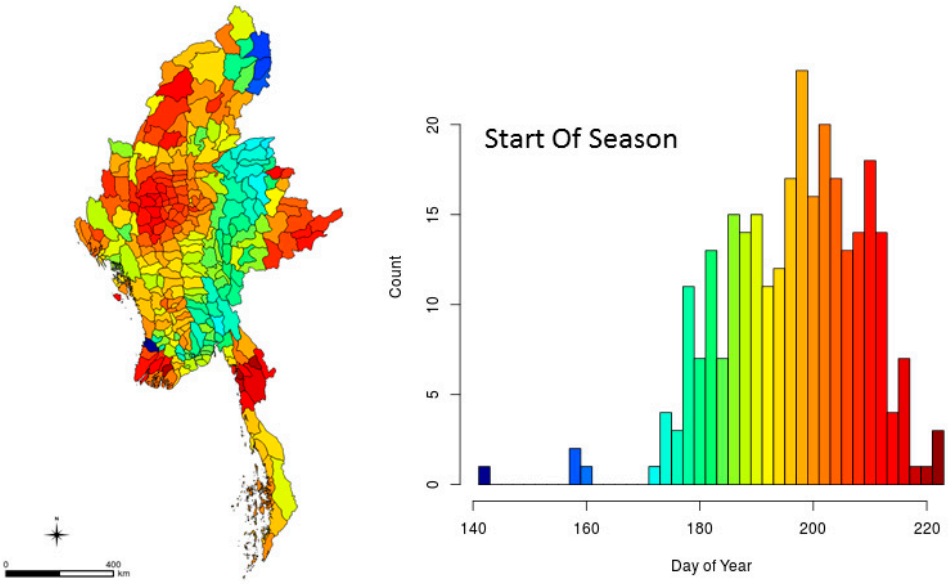

Figure 13. Rice crop start-of-season distribution across administrative units highlighting spatial variability and regional trends in crop calendar.

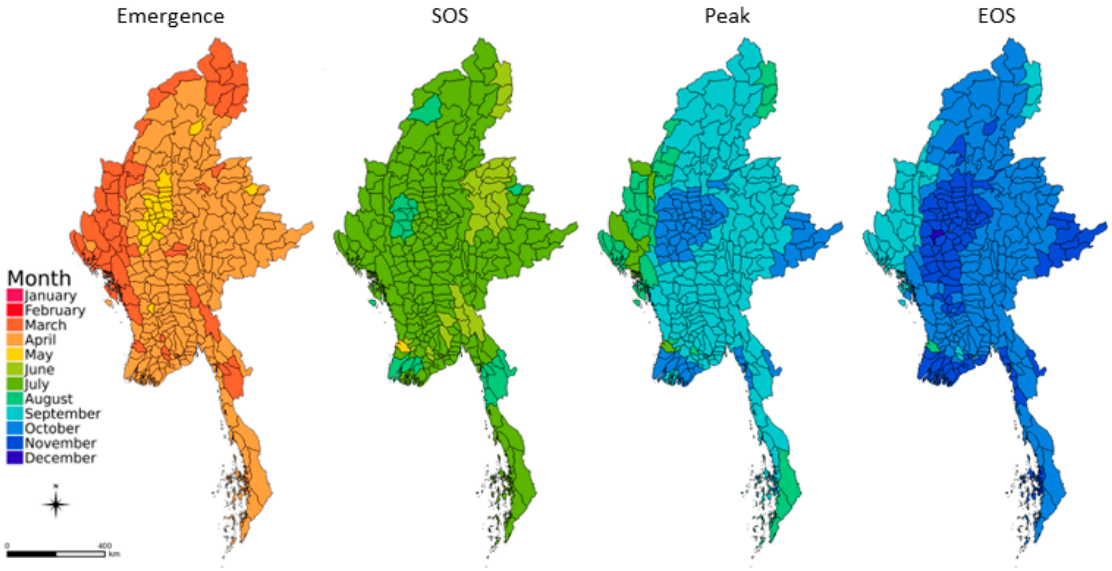

Figure 14. Rice crop calendar during the main wet season crop detected from Sentinel-1 showing mean A. Emergence, B. Start-of-season (SOS), C. Peak, and D. End-of-season (EOS) scaled to administrative units for Myanmar.

3.4. Comparison and Production Assessment

A scatterplot between our harvested area and the available rice census provided by the government at the State level is shown in Figure 15. While these outcomes need to be interpolated and used cautiously, the results indicated generally strong overall agreement with an R^2 of 0.78 using robust and transparent approach. Additional adjustments to the processing (i.e., masking, localized tuning) can improve the R^2, however this decreases the transferability of the approach. Incorporation of this type of approach into food security DSTs will need to weigh automation vs local tuning as part of their workflow. Further, we feel that the census statistics have such large uncertainty and production was affected by disaster flooding that the mapping approach provides a realistic assessment of rice production in Myanmar. The total harvested rice area was 6,652,111 ha which compares well to recent

FAO estimates and most recent IRRI MODIS-derived estimates (6,319,716 ha). However, the IRRI MODIS map does not integrate intensity so a direct comparison between extent and harvest area (extent × intensity) is in appropriate. Further, the IRRI MODIS data is from 2012 MODIS data at 500 m resolution and, we emphasize, detailed maps of the harvested area for Myanmar were not the primary objective of that IRRI effort. All these datasets provide valuable information for a given application. According to FAO Statistics, harvested rice has dropped nearly 20% from 2009 to 2014. Our 2015 Sentinel-derived operational estimates are within 2% of the 2014 estimates by the FAO. This is a difference of only 137,889 hectares. Further, in 2015, the FAO estimated a 3% reduction compared to 2014 due to flooding in July and August that negatively affected production.

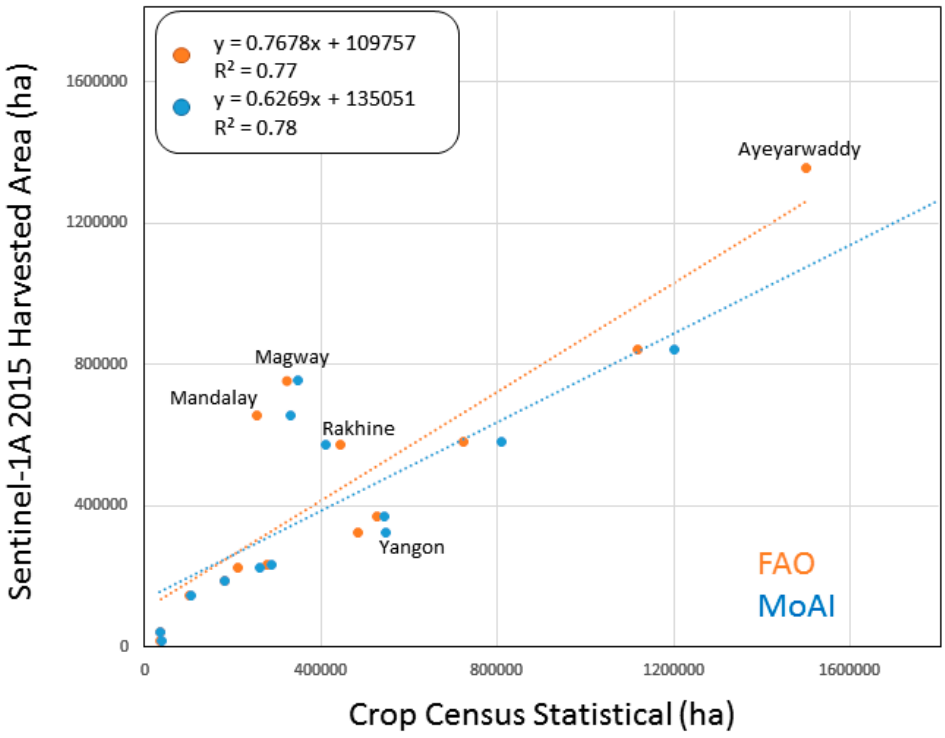

Figure 15. Scatterplot between 2015 census statistics and 2015 Sentinel-1A total harvested rice area shows moderate agreement with discrepancies due to Cyclone Komen disaster flooding and uncertainty in re-planting and accurate reporting.

4. Conclusions

This study highlights the strength of multi-sensor data integration for mapping broad land use land cover classes across a diverse landscape at moderate resolution. Fusing optical and microwave spectral regions provided very high overall accuracy and kappa outcomes over a large geographic region. For the first time, relatively high temporal frequency SAR over large geographic regions is made available at no cost. Phenological approaches applied to time series SAR allow for monitoring of rice agriculture with relevant information on extent, inundation, crop calendar, and intensity. The sensitivity of C-band SAR to rice crop development and temporally observing inundation and dynamic range are the main drivers to enabling accurate mapping of rice status information that is critical to food security programs such as AsiaRICE, FEWSNET, and GEOGLAM.

In reality, food security is complex and many factors are considered when making judgements on production and risks. The suite of rice information products generated in this research are one step closer toward more thorough and transparent monitoring. While the approach executed in this research application is scalable, more regions and validation will be required for implementation by existing DSTs. It is likely that each new geographic region will require tuning of algorithms to

its regional conditions. Unlike before, the availability of high frequency Sentinel-1 data now makes such applications feasible and provides for pathways towards operational monitoring over large areas in South and Southeast Asia at moderate spatial resolution. Further, "food security"—such as quantifying risks to production, estimating yield, assessment of drivers, developing adaptation strategies, mitigating impacts, and forecasting—are not individual "products" at this time created from Earth Observation data. These are complicated workflows involving many disciplines and international collaborations that can be improved with transparent, operational, and comprehensive information. Programs such as GEOGLAM and AsiaRice are working with communities on defining how the information is used, which thus influences how the data is developed. Using all the information in aggregate allows for more thoughtful decisions. Thus, having a suite of products on extent, calendar, hydroperiod, growth stage, and intensity allow more accurate and precise decisions. In general, the approach and outcomes in this research were transparent, robust, scalable, and could be implemented in a near real-time operational context, which are all wanted factors for food security programs. As the historical Sentinel-1 archives grow and more geographic regions are mapped, deviations from normal and or spatial variability will allow assessment and forecasting of production, which will add another layer of information for food security programs.

Lastly, government census statistics on crop production are challenging to obtain in Myanmar. While Ministries, such as Agriculture and Irrigation, have a Mission to promote food security, improve livelihoods, and implement sustainable growth, obtaining accurate and the latest census statistics is challenging. This emphasizes the need for initiatives, such as AsiaRice and GEOGLAM, to support food security in a transparent and open approach, and the need for satellite mapping tools to be able to monitor production or assess impacts of disasters. In countries such as Myanmar with large populations and GDP dependent upon rice production, more robust monitoring and assessment tools can help support better decision making and help normalize potential economic or political variables influencing census data or data access. The tools and flow described here are one example application on how SAR and multisensor crop mapping can be brought to scale for robust monitoring.

Acknowledgments: We thank three reviewers for their thoughtful comments that improved this research. Support for this work was provided in part by NASA Land Cover Land Use Change Program (MuSLI; NNX16AF96G) and SBIR (S5.02-9147). We thank NASA and USGS, ESA, and JAXA for providing Landsat-8, Sentinel-1, and PALSAR-2. Thanks to the NASA Land Cover Land Use Change (LCLUC) program for holding a regional workshop in Yangon, Myanmar.

Author Contributions: Nathan Torbick, Diya Chowdhury and William Salas conceived and designed the project; Diya Chowdhury and Nathan Torbick executed analyses; Jiaguo Qi provided assistance in regional coordination through MAIRS-FE; Nathan Torbick, Diya Chowdhury and William Salas wrote the paper.

Conflicts of Interest: The authors declare no conflict of interest. The funding sponsors had no role in the design of the study; in the collection, analyses, or interpretation of data; in the writing of the manuscript, and in the decision to publish the results.

References

1. Food and Agriculture Organization of the United Nations. Available online: http://www.fao.org/home/en (accessed on 15 September 2016).
2. Becker-Reshef, I.; Justice, C.; Sullivan, M.; Vermote, E.; Tucker, C.; Anyamba, A.; Small, J.; Pak, E.; Masuoka, E.; Schmaltz, J.; et al. Monitoring Global Croplands with Coarse Resolution Earth Observations: The Global Agriculture Monitoring (GLAM) Project. *Remote Sens.* **2010**, *2*, 1589–1609. [CrossRef]
3. Whitcraft, A.K.; Becker-Reshef, I.; Justice, C.O. A Framework for Defining Spatially Explicit Earth Observation Requirements for a Global Agricultural Monitoring Initiative (GEOGLAM). *Remote Sens.* **2015**, *7*, 1461–1481. [CrossRef]
4. Xiao, X.M.; Boles, S.; Liu, J.Y.; Zhuang, D.F.; Frolking, S.; Li, C. Mapping paddy rice agriculture in southern China using multi-temporal MODIS images. *Remote Sens. Environ.* **2005**, *95*, 480–492. [CrossRef]

5. Sakamoto, T.; Yokozawa, M.; Toritani, H.; Shibayama, M.; Ishitsuka, N.; Ohno, H. Spatio–temporal distribution of rice phenology and cropping systems in the Mekong Delta with special reference to the seasonal water flow of the Mekong and Bassac rivers. *Remote Sens. Environ.* **2006**, *100*, 1–16. [CrossRef]
6. Gumma, M.K.; Nelson, A.; Thenkabail, P.S.; Singh, A.N. Mapping rice areas in South Asia using MODIS multi temporal data. *J. Appl. Remote Sens.* **2011**, *5*, 053547. [CrossRef]
7. Torbick, N.; Salas, W.A.; Hagen, S.; Xiao, X. Mapping rice agriculture in the Sacramento Valley, USA with multitemporal PALSAR and MODIS imagery. *IEEE J. Sel. Top. Remote Sens.* **2010**, *4*, 451–457. [CrossRef]
8. Torbick, N.; Salas, W.; Xiao, X.; Ingraham, P.; Fearon, M.; Biradar, C.; Zhao, D.; Liu, Y.; Li, P.; Zhao, Y. Integrating SAR and optical imagery for regional mapping of paddy rice attributes in the Poyang Lake Watershed, China. *Can. J. Remote Sens.* **2011**, *37*, 17–26. [CrossRef]
9. Clauss, K.; Yan, H.; Kuenzer, C. Mapping Paddy Rice in China in 2002, 2005, 2010 and 2014 with MODIS Time Series. *Remote Sens.* **2016**, *8*, 434. [CrossRef]
10. Guan, X.; Huang, C.; Liu, G.; Meng, X.; Liu, Q. Mapping Rice Cropping Systems in Vietnam Using an NDVI-Based Time-Series Similarity Measurement Based on DTW Distance. *Remote Sens.* **2016**, *8*, 19. [CrossRef]
11. Biradar, C.M.; Xiao, X. Quantifying the area and spatial distribution of double- and triple-cropping croplands in India with multi-temporal MODIS imagery in 2005. *Int. J. Remote Sens.* **2011**, *32*, 367–386. [CrossRef]
12. Xiao, X.; Boles, S.; Frolking, S.; Li, C.; Babu, J.Y.; Salas, W.; Moore, B., III. Mapping paddy rice agriculture in South and Southeast Asia using multi-temporal MODIS images. *Remote Sens. Environ.* **2006**, *100*, 95–113. [CrossRef]
13. Thenkabail, P.S.; Biradar, C.M.; Noojipady, P.; Dheeravath, V.; Li, Y.J.; Velpuri, M.; Gumma, M.; Gangalakunta, O.R.P.; Turral, H.; Cai, X.L.; et al. Global irrigated area map (GIAM), derived from remote sensing, for the end of the last millennium. *Int. J. Remote Sens.* **2009**, *30*, 3679–3733. [CrossRef]
14. Gumma, M.K.; Thenkabail, P.S.; Maunahan, A.; Islam, S.; Nelson, A. Mapping seasonal rice cropland extent and area in the high cropping intensity environment of Bangladesh using MODIS 500 m data for the year 2010. *ISPRS J. Photogramm.* **2014**, *91*, 98–113. [CrossRef]
15. Rojas, O.; Vrieling, A.; Rembold, F. Assessing drought probability for agricultureal areas in Africa with coarse resolution remote sensing imagery. *Remote Sens. Environ.* **2011**, *115*, 343–352. [CrossRef]
16. Torbick, N.; Salas, W. Mapping agricultural wetlands in the Sacramento Valley, USA with satellite remote sensing. *Wetl. Ecol. Manag.* **2014**, *23*, 79–94. [CrossRef]
17. Dong, J.; Xiao, X.; Kou, W.; Qin, Y.; Zhang, G.; Li, L.; Jin, C.; Zhou, Y.; Wang, J.; Biradar, C.; et al. Tracking the dynamics of paddy rice planting area in 1986–2010 through time series Landsat images and phenology-based algorithms. *Remote Sens. Environ.* **2015**, *160*, 99–113. [CrossRef]
18. Zhou, Y.; Xiao, X.; Qin, Y.; Dong, J.; Zhang, G.; Kou, W.; Jin, C.; Wang, J.; Li, X. Mapping paddy rice planting area in rice-wetland coexistent areas through analysis of Landsat 8 OLI and MODIS images. *Int. J. Appl. Earth Obs.* **2016**, *46*, 1–12. [CrossRef] [PubMed]
19. Chen, C.; McNairn, H. A neural network integrated approach for rice crop monitoring. *Int. J. Remote Sens.* **2006**, *27*, 1367–1393. [CrossRef]
20. Inoue, Y.; Kurosu, T.; Mseno, H.; Uratsuka, S.; Kozu, T.; Dabrowska-Zielinska, K.; Qi, J. Season-long daily measurements of multifrequency (Ka, Ku, X, C, and L) and full-polarizaiton backscatter signatures over paddy rice field and their relationship with biological variables. *Remote Sens. Environ.* **2002**, *81*, 194–204. [CrossRef]
21. Le Toan, T.; Ribbes, F.; Wang, L.F.; Floury, N.; Ding, K.H.; Kong, J.A.; Fujita, M. Rice Crop Mapping and Monitoring Using ERS-1 Data Based on Experiment and Modeling Results. *IEEE Trans. Geosci. Remote* **1997**, *35*, 41–56. [CrossRef]
22. Ribbes, F.; Le Toan, T. Rice parameter retrieval and yield prediction using radarsat data. In *Towards Digital Earth*; International Symposium in Digital Earth: Toulouse, France, 1999.
23. Bouvet, A.; Le Toan, T.; Lam-Dao, N. Monitoring of the rice cropping system in the Mekong Delta using ENVISAT/ASAR dual polarization data. *IEEE Trans. Geosci. Remote* **2009**, *47*, 517–526. [CrossRef]
24. Kuenzer, C.; Knauer, K. Remote sensing of rice crop areas. *Int. J. Remote Sens.* **2013**, *34*, 2101–2139. [CrossRef]
25. Inoue, Y.; Sakaiya, E.; Wang, C. Capability of C-band backscattering coefficients from high-resolution satellite SAR sensors to assess biophysical variables in paddy rice. *Remote Sens. Environ.* **2014**, *140*, 257–266. [CrossRef]

26. Nelson, A.; Setiyono, T.; Rala, A.B.; Quicho, E.D.; Raviz, J.V.; Abonete, P.J.; Maunahan, A.A.; Garcia, C.A.; Bhatti, H.Z.M.; Villano, L.S.; et al. Towards an Operational SAR-Based Rice Monitoring System in Asia: Examples from 13 Demonstration Sites across Asia in the RIICE Project. *Remote Sens.* **2014**, *6*, 10773–10812. [CrossRef]
27. Torres, R.; Snoeij, P.; Geudtner, D.; Bibby, D.; Davidson, M.; Attema, E.; Potin, P.; Rommen, B.; Floury, N.; Brown, M.; et al. GMES Sentinel-1 mission. *Remote Sens. Environ.* **2012**, *120*, 9–24. [CrossRef]
28. Torbick, N.; Salas, W.; Chowdhury, D.; Ingraham, P. Mapping rice greenhouse gas emissions in the Red River Delta Vietnam. *Carb. Manag.* **2017**, in press.
29. United States Department of Agriculture Foreign Agricultural Service. Available online: http://www.fas.usda.gov (accessed on 9 September 2016).
30. Roy, D.P.; Wulder, M.A.; Loveland, T.R.; Woodcock, C.E.; Allen, R.G.; Anderson, M.C.; Scambos, T.A. Landsat-8: Science and product vision for terrestrial global change research. *Remote Sens. Environ.* **2014**, *145*, 154–172. [CrossRef]
31. Vermote, E.; Justice, C.; Claverie, M.; Franch, B. Preliminary analysis of the performance of the Landsat 8/OLI land surface reflectance product. *Remote Sens. Environ.* **2016**, *185*, 46–56. [CrossRef]
32. Masek, J.G.; Vermote, E.F.; Saleous, N.E.; Wolfe, R.; Hall, F.G.; Huemmrich, K.F.; Gao, F.; Kutler, J.; Lim, T.K. A Landsat surface reflectance dataset for North America, 1990–2000. *IEEE Geosci. Remote Sens. Soc.* **2006**, *3*, 68–72. [CrossRef]
33. Vermote, E.F.; El Saleous, N.; Justice, C.O.; Kaufman, Y.J.; Privette, J.L.; Remer, L.; Roger, J.C.; Tanré, D. Atmospheric correction of visible to middle-infrared EOS-MODIS data over land surfaces: Background, operational algorithm and validation. *J. Geophys. Res.-Atmos.* **1997**, *102*, 17131–17141. [CrossRef]
34. Zhu, Z.; Woodcock, C.E. Object-based cloud and cloud shadow detection in Landsat imagery. *Remote Sens. Environ.* **2012**, *118*, 83–94. [CrossRef]
35. Vermote, E.F.; Kotchenova, S. Atmospheric correction for the monitoring of land surfaces. *J. Geophys. Res.-Atmos.* **2008**, *113*. [CrossRef]
36. Irish, R.R.; Barker, J.L.; Goward, S.N.; Arvidson, T. Characterization of the Landsat 7 ETM+ automated cloud cover assessment (ACCA) algorithm. *Photogramm. Eng. Remote Sens.* **2006**, *72*, 1179–1188. [CrossRef]
37. Rouse, J.W., Jr.; Haas, R.H.; Schell, J.A.; Deering, D.W. Monitoring vegetation systems in the Great Plains with ERTS. In Proceedings of the Third ERTS Symposium, Washington, DC, USA, 10 December 1974; Freden, S.C., Mercanti, E.P., Becker, M.A., Eds.; pp. 309–317.
38. Tucker, C.J. Red and photographic infrared linear combinations for monitoring vegetation. *Remote Sens. Environ.* **1979**, *8*, 127–150. [CrossRef]
39. Xiao, X.; Boles, S.; Liu, J.; Zhuang, D.; Liu, M. Characterization of forest types in Northeastern China, using multi-temporal SPOT-4 VEGETATION sensor data. *Remote Sens. Environ.* **2002**, *82*, 335–348. [CrossRef]
40. Hagen, S.; Heilman, P.; Marsett, R.; Torbick, N.; Salas, W.; van Ravensway, J.; Qi, J. Mapping total vegetation cover across western rangelands with MODIS data. *Rangel. Ecol. Manag.* **2012**, *65*, 456–467. [CrossRef]
41. Xiao, X.; Dorovskoy, P.; Biradar, C.; Bridge, E. A library of georeferenced photos from the field. *EOS Earth Space Sci.* **2011**, *92*, 453–454. [CrossRef]
42. Torbick, N.; Ledoux, L.; Salas, W.; Zhao, M. Regional Mapping of Plantation Extent Using Multisensor Imagery. *Remote Sens.* **2016**, *8*, 236. [CrossRef]
43. Breiman, L. Random Forests. *Mach. Learn.* **2001**, *45*, 5–32. [CrossRef]
44. Lawrence, R.L.; Wood, S.D.; Sheley, R.L. Mapping invasive plants using hyperspectral imagery and Breiman cutler classifications (randomForest). *Remote Sens. Environ.* **2006**, *100*, 356–362. [CrossRef]
45. Watts, J.D.; Lawrence, R.L.; Miller, P.R.; Montagne, C. Monitoring of cropland practices for carbon sequestration purposes in north central Montana by Landsat remote sensing. *Remote Sens. Environ.* **2009**, *113*, 1843–1852. [CrossRef]
46. Schultz, B.; Immitzer, M.; Formaggio, A.R.; Sanches, I.D.A.; Luiz, A.J.B.; Atzberger, C. Self-guided segmentation and classification of multi-temporal Landsat 8 images for crop type mapping in southwestern Brazil. *Remote Sens.* **2015**, *7*, 14482–14508. [CrossRef]
47. Whitcomb, J.; Moghaddam, M.; McDonlad, K.; Kellndorfer, J.; Podest, E. Mapping vegetated wetlands of Alaska using L-band radar satellite imagery. *Can. J. Remote Sens.* **2009**, *35*, 54–72. [CrossRef]
48. Torbick, N.; Persson, A.; Olefeldt, D.; Frolking, S.; Salas, W.; Hagen, S.; Crill, P.; Li, C. High resolution mapping of peatland hydroperiod at a high-latitude Swedish mire. *Remote Sens.* **2012**, *4*, 1974–1994. [CrossRef]

49. Wilkes, P.; Jones, S.D.; Suarez, L.; Mellor, A.; Woodgate, W.; Soto-Berelov, M.; Haywood, A.; Skidmore, A.K. Mapping forest canopy height over large areas by upscaling ALS estimates with freely available satellite data. *Remote Sens.* **2015**, *7*, 12563–12587. [CrossRef]
50. Song, W.; Dolon, J.M.; Cline, D.; Xiong, G. Leanring-based algal bloom event recognition for oceanographic decision support system using remote sensing data. *Remote Sens.* **2015**, *7*, 13564–13585. [CrossRef]
51. Torbick, N.; Corbiere, M. Mapping urban sprawl and impervious surfaces in the northeast United States for the past four decades. *GISci Remote Sens.* **2015**, *52*, 746–764. [CrossRef]
52. Karlson, M.; Ostwald, M.; Reese, H.; Sanou, J.; Tankoano, B.; Mattsson, E. Mapping tree canopy cover and aboveground biomass in Sudano-Sahelian woodlands using Landsat 8 and random forest. *Remote Sens.* **2015**, *7*, 10017–10041. [CrossRef]
53. Nguyen, D.B.; Gruber, A.; Wagner, W. Mapping rice extent and cropping scheme in the Mekong Delta using Sentinel-1A data. *Remote Sens. Lett.* **2016**, *7*, 1209–1218. [CrossRef]
54. Savitzky, A.; Golay, M.J.E. Smoothing and Differentiation of Data by Simplified Least Squares Procedures. *Anal. Chem.* **1964**, *36*, 1627–1639. [CrossRef]
55. Whittaker, E.T.; Robinson, G. The Calculus of Observations. *Trans. Fac. Act.* **1924**, *10*, 1924–1925.
56. Atzberger, C.; Eilers, P.H.C. A time series for monitoring vegetation activity and phenology at 10-daily time steps covering large parts of South America. *Int. J. Dig. Earth* **2011**, *4*, 365–386. [CrossRef]
57. Atkinson, P.M.; Jeganathan, C.; Dash, J.; Atzberger, C. Inter-comparison of four models for smoothing satellite sensor time-series data to estimate vegetation phenology. *Remote Sens. Environ.* **2012**, *123*, 400–417. [CrossRef]
58. Eilers, P.H.C. A Perfect Smoother. *Anal. Chem.* **2003**, *75*, 3631–3636. [CrossRef] [PubMed]
59. Inglada, J.; Vincent, A.; Arias, M.; Marais-Sicre, C. Improved Early Crop Type Identification By Joint Use of High Temporal Resolution SAR And Optical Image Time Series. *Remote Sens.* **2016**, *8*, 362. [CrossRef]